Proceedings of the 3rd World Congress on Mechanical, Chemical, and Material Engineering (MCM'17)
Rome, Italy – June 8 – 10, 2017
Paper No. HTFF 116
ISSN: 2369-8136
DOI: 10.11159/htff17.116

The Reynolds Stresses Equation Modelling in the Prediction of Flow Past a Rotating Cylinder at High Reynolds Number

Sitthichai Ruchayosyothin, Tim J. Craft, Hector Iacovides
School of Mechanical Aerospace and Civil Engineering, University of Manchester
Manchester, M13 9PL, UK
sitthichai.ruchayosyothin @postgrad.manchester.ac.uk; tim.craft@manchester.ac.uk; h.iacovides@manchester.ac.uk

Abstract **-** This research presents the predictions of flow past a rotating cylinder at a subcritical Reynolds number of 130,000. The main objective is to identify turbulence effective modelling strategies for unsteady RANS computations. For this reason both effective-viscosity and stress-transport models have been used with different strategies for the modelling of near-wall turbulence which include standard log-law-based, and more refined wall functions, the latter based on the analytical solution of 1-D equations for the transport of wall-parallel momentum. The models' effectiveness is assessed through comparisons with available experimental and Large Eddy Simulation (LES) data. It is important that these present studies are in a good agreement with those obtained by the decreasing drag coefficient and increasing lift coefficient when a spin ratios (α : proportional tangential velocity of the cylinder wall to inlet flow velocity) of a cylinder grow up. Moreover, the stability of the flow domain is well improved with the suppressed vortex shedding, as well. Significantly, the prediction of the position of stagnation and separation flow position correspond to the magnitude of lift, drag coefficient and the rotation direction. Overall, this research has confirmed that the RSMs is capable to examine the external flow and more sensitized on the curvature surface flow.

Keywords**:** Reynolds stresses equation model, linear k-ε, rotating cylinder, Magnus effect, high Reynolds number, rotating cylinder, turbulence modelling

1. Introduction

Flow across cylinders is of relevance to a wide range of applications and flow across rotating cylinders in particular, following the findings of Magnus [1], has attracted the interest of aerodynamicists. Magnus [1] ,in 1853, showed that because in flows across rotating cylinders the flow and pressure distributions around the cylinder are no longer symmetric, the resulting force exerted by the fluid on the cylinder has components in the direction parallel to the flow direction (the drag force) and also in the direction normal to the flow direction (the lift force). Magnus's [1] initial research was largely qualitative. Several experimental and computational investigations have appeared since then, aiming to provide quantitative information

Starting with laminar flow, Coutancea and Monard [2] have conducted an experimental investigation of flow past a cylinder, at a Reynolds number of 200 and spin ratios ($\alpha = \omega D/2U_\infty$) of 0 to 3.5. For the stationary cylinder they showed that a large and unsteady, but on average symmetric, recirculation region is formed over the downstream half of the cylinder. At low spin ratios the recirculation region remain large and unsteady, while higher spin ratios stabilized the recirculation regions, reduced it in size and displaced it circumferentially along the direction of rotation. Subsequently Badr and Dennis [3] showed that 2-D unsteady laminar flow predictions are in good agreement with the data. Neither of these two studies, [2] and [3] , however, reported the values of the aerodynamic forces. Mittal and Kumar [4], on the other hand, who also conducted a numerical investigation of laminar flow past a rotating cylinder, included information on the effects of the spin ratio on the lift and drag coefficients. It was demonstrated that while the lift coefficient increased with spin ratio, the drag coefficient showed a steep reduction. Moreover, it was shown that at spin ratios greater than 1.9, the vortex shedding behind the cylinder is suppressed.

Brede et al.[5] focused on flow instabilities in flows past rotating cylinders by using PIV (particle image velocimetry) technique to capture the flow field. Vortex shedding was observed to occur because small eddies separated from the cylinder surface and interacted with the main flow. For the case of stationary cylinder, the numerical study of Braza et al.

[6] shows that for Reynolds number greater than 200, the dimensionless vortex shedding frequency is around 0.21, while the numerical study of Gushchin et al. [7] shows that for spheres this frequency is lower.

In case of turbulence flow, Cantwell and Coles [8] and Norberg [9], presented experimental studies of flows past stationary cylinders, at Reynolds numbers of 140,000 and 200,000, respectively. Their results provided better understanding of the influence of Reynolds number and of inlet turbulence intensity on the flow development. Maximum turbulence levels were measured within the re-circulation region at the back of the cylinder, the wake distance inversely related with drag coefficient and turbulence intensity at the same Reynolds number. These researches also showed the velocity along flow direction and pressure distribution around a circular cylinder. These experimental results were subsequently employed as validation data in LES [10] and URANS [11] numerical studies.

For turbulent flows over rotating cylinders, Aokii and Ito [12], carried out an experimental investigation for Reynolds numbers up to 130,000 and spin ratios up to 1.2. The data presented includes variation of lift and drag coefficients with spin ratio, variation of the Strouhal number of vortex shedding with spin ratio and also velocity profiles downstream of the cylinder. The resulting data provide interesting insights in the effects of cylinder rotation, but for the Reynolds number of 130,000 they only extent to spin rations less than 0.5. URANS predictions based on the RNG version of the k-ε model were also included which showed considerable deviations from the measurements. The aerodynamic behaviour, variation in lift and drag coefficients, of rotating cylinders in cross-flow, has also been experimentally investigated by Reid [13], Swanson [14] and Clayton [15]. These investigations covered a range of Reynolds numbers from 92,000 to 500,000 and spin ratios up to 4.32. Their works have confirmed that at high spin ratios the lift coefficient increases and the drag coefficient goes down, while at values less than 1 there is a sudden drop in the value of the lift coefficient, attributed to transition.

Some computational studies focus on flow across rotating cylinders at Reynolds number values of 130,000-140,000 and at several spin ratios. The related turbulence models are standard k-ε [16], RNG k-ε [12], LES [10], DES [17] and PANS [18]. These computational researches reported information which earlier experimental studies did not include, such as, the displacement of the stagnation and separation points under rotating conditions. This information helps to explain how rotation influences the aerodynamic characteristics. Some of the models employed in the earlier studies displayed major predictive weaknesses, while the more accurate LES approach involves high computational costs. The purpose of this study is to apply a number of approaches to the modelling of the turbulent stresses in general and also to the modeling of the near-wall turbulence, in flow computations across stationary and rotating cylinders and to assess their predictive effectiveness.

Abbreviations / Nomenclatures

DES detached eddy simulation	P, p' mean and fluctuation pressure	$C_{\varepsilon 1}$,$C_{\varepsilon 2}$ constant of ε eq. (1.44, 1.92)
PANS partially averaged Navier-Strokes	ρ density	$\sigma^{(k)}$ turbulent Prandl number (1.0)
DNS direct numerical method	μ,ν kinetic and dynamic viscosity	f_1, f_2 closure coefficient of ε eq. (1,1)
RNG renormalization group	x_i, x_j, x_k coordinate of 1st,2nd, 3rd axis	S_l, S_ε length scale and ε source term
U_i component velocity	δ_{ij} Kronecter delta 1(i=j) or 0 (i≠j)	y, y^+ non / dimensionless wall distance
f vortex shedding frequency	c_s diffusion process coefficient (0.22)	c_1, c_2 constant for RSMs (1.8, 0.6)
$\bar{}$ average	c_μ, eddy diffusivity coefficient (0.09)	c_{1w},c_{2w} constant for RSMs (0.5,0.3)
$\square_t$ turbulence	f_μ damping factor	i,j,k,l,m matrix or stress tensor
P_k turbulence generation rate	ω angular cylinder velocity	n normal unit vector
U_∞ free stream velocity	D cylinder diameter	

Therefore, here both effective-viscosity and second-moment closure models are tested for the modeling of the turbulent stresses. For the modeling of the effects of the near-wall turbulence, both the "standard", log-law-based, wall function , WF, and the more refined analytical wall function, AWF, have been tested. The objective is, through comparisons with available experimental and LES/DNS data, to identify RANS models which can reliably predict the aerodynamics of flows across both stationary and spinning cylinders.

2. Turbulence Modelling

Within the unsteady Reynolds averaged Navier-Strokes (U-RANS) approach the transport equations for the time-averaged momentum adopt the form:

$$\frac{\partial \overline{U}_i}{\partial t} + \frac{\partial (\overline{U}_i \overline{U}_j)}{\partial x_j} = -\frac{1}{\rho}\frac{\partial P}{\partial x_i} + \frac{\partial}{\partial x_j}\left(\nu \frac{\partial \overline{U}_i}{\partial x_j} - \overline{u_i' u'_j} \right) \tag{1}$$

Where $\overline{U}_i$ denotes the time averaged velocity component and u_i' is the instantaneous fluctuation one. The second moment of the fluctuating velocity , ($u'_i u'_j$), which appear in equation (1) above, also known as the Reynolds or turbulent stresses, are unknown and their distribution within the flow field needs to be approximated through the introduction of the turbulence modelling equations,

Within the effective viscosity approximation the Reynolds stresses are assumed to depend linearly on the mean strain rate through equations (2) and (3):

$$\overline{u_i u_j} = \frac{2}{3} k \delta_{ij} - \nu_t \left(\frac{\partial \overline{U}_i}{\partial x_j} + \frac{\partial \overline{U}_j}{\partial x_i} \right) \tag{2}$$

$$\nu_t = C_\mu f_\mu \frac{k^2}{\varepsilon} \tag{3}$$

Where k and ε, are the turbulent kinetic energy and its dissipation rate which are obtained from separate transport equations.

The more elaborate Reynolds stress equation model, involves the solution of separate transport equations for each component of the Reynolds stress tensor, as shown in equation (4) below:

$$\frac{\partial}{\partial t}(\rho \overline{u_i' u_j'}) + \frac{\partial}{\partial x_k}(\rho \overline{U}_k \overline{u_i' u_j'}) = \frac{\partial}{\partial x_k} d_{ijk} + \rho (P_{ij} + \Phi_{ij} - \varepsilon_{ij}) \tag{4}$$

The terms on the left hand side of equation (4) and also the generation rate term, Pij, defined below, on the right hand side are exact

$$P_{ij} = -\left(\overline{u_i' u_k'} \frac{\partial \overline{U}_j}{\partial x_k} + \overline{u_j' u_k'} \frac{\partial \overline{U}_i}{\partial x_k} \right) \tag{5}$$

The remaining terms on the right hand side require modelling. The term Φ_{ij}, is a redistributive term ($\Phi_{11}+\Phi_{22}+\Phi_{33}=0$) and represents the effect of the interaction between the pressure and strain fluctuations. The first element in equation (6) is a linear approximation to the isotropization of the Reynolds stresses driven by the stress anisotropy and the second is also a linear approximation of the isotropization of the generation rate of the turbulent stresses. The last two terms are only active near the walls and remove energy from fluctuations in the wall-normal direction and redistribute it to the wall-parallel directions

$$\begin{aligned} \Phi_{ij} = -c_1 \varepsilon a_{ij} - c_2 \left(P_{ij} - \frac{1}{3} P_{kk} \delta_{ij} \right) + c_{1w} \frac{\varepsilon}{k} \left(\overline{u_l' u'_m} n_l n_m \delta_{ij} - \frac{3}{2} \overline{u_i' u'_m} n_j n_l - \frac{3}{2} \overline{u_j' u'_l} n_i n_l \right) \left(\frac{\iota}{2.5y} \right) \\ + c_{2w} \frac{\varepsilon}{k} \left(\phi_{lm2} n_l n_m \delta_{ij} - \frac{3}{2} \phi_{li2} n_l n_j - \frac{3}{2} \phi_{lj2} n_l n_i \right) \left(\frac{\iota}{2.5y} \right) \end{aligned} \tag{6}$$

where the Reynolds stress anisotropic tensor (a_{ij}) as $a_{ij} = \frac{\overline{u_i' u_j'}}{k} - \frac{2}{3}\delta_{ij}$, ϕ_{ijk} is the total flux and ι is the turbulence length scale, defined as $\frac{k^{\frac{3}{2}}}{\varepsilon}$

The viscous dissipation rate of each stress component (ε_{ij}) is;

$$\varepsilon_{ij} = \nu \frac{\partial u_i'}{\partial x_j} \frac{\partial u_j'}{\partial x_i} \approx \frac{2}{3}\varepsilon\delta_{ij} \tag{7}$$

The term d_{ijk} represents the transport of the stresses through turbulent mixing, first three elements in equation (8) and viscous diffusion.

$$d_{ijk} = -\rho\overline{u_i' u_j' u_k'} - \overline{p' u_j'}\delta_{ik} - \overline{p' u_i'}\delta_{jk} + \mu \frac{\partial \overline{u_i' u_j'}}{\partial x_k} \tag{8}$$

The turbulent transport is modeled through the generalized gradient diffusion hypothesis (GGDH) of Daly and Harlow[19], while the viscous diffusion is exact, so equation (8) becomes:

$$d_{ijk} = c_s \rho \frac{k}{\varepsilon} u_k' u_l' \frac{\partial \overline{u_i' u_j'}}{\partial x_l} + \mu \frac{\partial \overline{u_i' u_j'}}{\partial x_k} \tag{9}$$

The dissipation rate of the turbulent kinetic energy, ε, which appears in equation (7), is obtained from equation (10) below.

$$\frac{\partial}{\partial t}(\rho\varepsilon) + \frac{\partial}{\partial x_i}(\rho \overline{U}_i \varepsilon) = \frac{\partial}{\partial x_i}\left[(\mu + \frac{\mu_t}{\sigma^{(\varepsilon)}})\frac{\partial \varepsilon}{\partial x_i}\right] + \rho\left(C_{\varepsilon 1} f_1 P_k - C_{\varepsilon 2} f_2 \varepsilon\right)\frac{\varepsilon}{k} + \rho(S_l + S_\varepsilon) \tag{10}$$

where $P_k = \frac{1}{2}P_{ii}$ and all constants proposed in Gibson and Launder [20]. Both models mentioned here are of the high-Reynolds-number type, which means that they cannot be extended to regions in which the turbulent length scales become small, like the wall viscous sub-layer. To overcome this limitation the most popular approach is to employ the wall function strategy. The near-wall control volume is large enough for the near-wall node to be outside the viscous sub-layer. Within the originally proposed, conventional strategy, referred to here as WF, the assumption of a logarithmic near-wall velocity distribution is used to relate the value of the wall shear stress to that of the wall-parallel velocity at the near-wall node. Here, in addition to the conventional approach ,a more refined one, developed by the Manchester group, [21] has been tested, the AWF. In this approach, the value of the wall shear stress is related to that of the wall-parallel velocity at the near-wall node, through the analytical solution of a simplified 1-dimemsional transport equation for the wall parallel momentum.

3. Numerical Method

Here we use the 'STREAM' code which is an in-house CFD (the computational fluid dynamic) solver which uses the finite volume approach to descretize the momentum transport equation, using Cartesian decomposition, for non-orthogonal structured grids [22]. For stability, the upwind different scheme (UPWIND), is used for the descretization of the convective transport of the turbulence parameters and the third order upstream monotonic interpolation for scalar transport

scheme (UMIST) is used for the desrcitization of the convective transport of the mean momentum equations. For the temporal discretization the 2nd-order Crank-Nicholson method is employed. The pressure velocity coupling is handled through the use of the well known SIMPLE algorithm with the Rhie and Chow flux interpolation used to remove pressure chequer-boarding associated with the collocation of velocity and scalar nodes.

3.1. Cases Examined

All the cases computed here have been assumed to be 3-dimensional and time-dependent. The cylinders are assumed to be infinitely long and in order to capture large-scale 3-dimensional structures a cylindrical flow domain is being considered, with the solid cylinder at its centre, whose diameter is 10 times greater and its length two times longer than the cylinder diameter. In order to reproduce the conditions of experimental studies such as those of Aoki and Ito [12], the Reynolds number, based on free stream velocity and cylinder diameter ($Re=U_\infty D/\nu$) varies between 130,000 and 140,000 and the spin ratio range is from 0 (stationary) to 5.

3.2. Computational Domain

A cylindrical mesh is used to resolve the solution domain consisting of 300×240×20 nodes in the radial, circumferential and axial directions respectively. The non-uniformity of the grid in the radial direction is increased at higher spin ratios, in order maintain adequate resolution of turbulent boundary layer around the cylinder, which becomes thinner at higher spin rates. Over the upstream half of the outer circumferential boundary a uniform free stream velocity is prescribed. The level of the turbulent intensity is set to 1% and the dissipation rate is set to a value which results in the turbulent viscosity being 10 times higher than the molecular viscosity, over the same part of the outer circumferential boundary. Over the downstream half of the outer boundary, exit conditions are prescribed, with uniform exit pressure. In the axial direction, periodic flow boundary conditions are imposed. The time step, Δt, is set so that $\Delta t < \Delta x/U_\infty D$.

4. Results and Discussion

The assessment of the models effectiveness starts with flow across stationary cylinders. In Table 1, the values of the Lift and Drag Coefficients and also those of the dimensionless frequency, Strouhal number ($St=fD/U_\infty$) of the vortex shedding behind the cylinder computed in the present study, are compared with those determined either experimentally, or in earlier LES and hybrid RANS/LES studies. The computation of zero time-averaged values for the lift coefficient confirms that for stationary cylinders in cross flow, the predicted time-averaged flow field is symmetric. For the lift coefficient, the results of the earlier studies [12], [10], [17], [18] and [16] show that there is close agreement between the experimental and LES values, but the high-Re k-ε employed in reference [16], severely under-predicted the level of the drag coefficient by a factor of 2. This suggests that this model delays the prediction of flow separation downstream of the cylinder and consequently under-estimates the size of the downstream wake. The hybrid LES/RANS methods of references [17] and [18] also under-estimate the value of the drag coefficient, which suggests that the RANS models employed have similar predictive weaknesses as the high-Re k-ε. Turning the attention to the computations of this study, the first observation to note, is that they confirm the high-Re k-ε / WF model C_D predictions of reference [16]. Replacing the log-law-based wall function, WS, with the more refined analytical version, AWF, lead to substantial improvements, almost halving the difference between the measured and predicted C_D values, though of course this still leaves room for improvement. Nevertheless, the conclusion is that less empirical analytical wall function is more appropriate for the prediction of flow separation. The introduction of the second-moment closure, in place of the effective-viscosity model, however, results in greater a predictive improvement in the value of the drag coefficient which brings it to close (12%) agreement with the experimental value. Moreover, replacing the log-low-based wall function, WS, with the analytical version, AWF, in combination with the second-moment closure, results in additional predictive improvements, which reduces the gap between predictions and measurements to <8%. The corresponding Strouhal number comparisons, also included in Table 1, lead to conclusions similar to those reached in the drag force comparisons.

Table 1: The aerodynamic of flow past a stationary cylinder at Re. 130,000 - 140,000.

Aerodynamic Result	Experiments	LES [10]	DES [17]	PANS [18]	k-ε -WF [16]	Present Studies			
						RSMs WF	RSMs AWF	k-ε WF	k-ε AWF
C_L	0 [12]	0	0	0	0	0	0	0	0
C_D	1.15 [12]	1.03	0.65	0.62	0.56	1.29	1.24	0.59	0.79
St	0.18 [8]	-	0.28	0.27	-	0.24	0.22	0.31	0.28

The plots of the predicted time histories of the lift coefficient at different spin ratios, presented in Figure 1 provide a first view of the overall effect of spin ratio on the lift force and also highlights the predictive differences of the different modelling strategies. All models indicate that there is a continuous increase in lift force with spin ratio. Flow oscillations are predicted to be strong at stationary conditions (spin ratio of zero) and to entirely diminish by the time the spin ratio reaches the value of 3. Changing either from an effective-viscosity model to a second –moment closure, or from a standard, log-law-based wall function to a more advanced analytical wall function, leads to the prediction of stronger flow fluctuations.

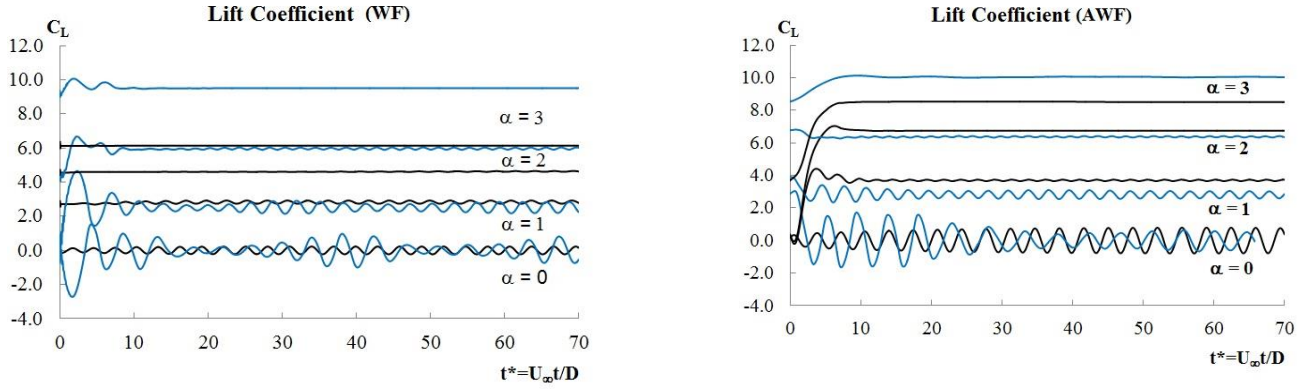

Fig. 1: The time history of lift coefficient of (–) linear k-ε and (–) RSMs with (left) WF and (right) AWF.

Figure 2 presents comparisons of predicted and measured lift and drag coefficients over a range of spin ratios. They provide the opportunity to assess the models' ability to predict the aerodynamic characteristics of rotating cylinders. As far as the lift coefficient is concerned, there experimental data [12] and [13], which extend to spin ratio values greater than 4 and the LES data [10], are in close agreement, showing values of practically zero for α values up to 0.5 and subsequently a monotonic rise with the lift coefficient becoming as high as 10 at a spin ratio of 5. In the case of the drag coefficient on the other hand, whole both the experiments and the LES data display an initial reduction in CD with spin ratio up to α=1, beyond this point while the experimental data show an increase in the drag coefficient, the LES data suggest that the drag coefficient continues to fall at higher spin ratios becoming practically zero. It should also be noted that even the experimental, higher, CD values at higher spin ratios are considerably (nearly an order of magnitude) lower than the corresponding lift coefficient levels. At spin ratios higher than 0.5, all current predictions, return an overall variation in the lift coefficient similar to that of the experiments. While the differences in the CL values predicted by the different models are modest, at spin ratios lower than 2.5 the second-moment-closure predicted CL levels are closer to those measured, while at higher spin levels the CL values returned by the k-ε/AWF model are closer. As already commented, at stationary conditions there is a wide variation in the predicted values of the drag coefficient, with the second-moment closures being close to the measured value and the k-ε models severely under-estimating it. These predictive differences among the models gradually diminish as the spin ratio is increased. This is probably caused by the fact that rotation suppresses the downstream wake, which is the flow feature that effective-viscosity models fail predict correctly. At the higher spin ratios the models predict low values of CD, which are in agreement with the LES predictions but in contrast to the experimental data.

A possible explanation for the under predicted drag coefficient are shown in Figure 3. The major evidence of resulting force coefficient (CF) has a similar trend and closing value with lift coefficient in Figure 2 as entire spin ratios. It implies

that the lift force (FL) is the most influent on the total aerodynamic force, whilst the drag force (FD) has smaller scale when comparing with the lift force. Moreover, the direction of the resulting force has a significant effect on the drag coefficient. For example, although RSMs-WF prediction has a little different angle around 7.89° or 9.65%, the prediction in drag coefficient result in under prediction by 1.25 or 92.59% as spin ratio of 4.

Figure 4 demonstrates the time-averaged pressure coefficient (Cp) distribution around the middle plane of the cylinder at spin ratios of 0 and 2. The results show symmetric distribution around the stationary cylinder, and asymmetric around the rotating cylinder. In the stationary cylinder case, all the data agree that the stagnation point is at the front of the cylinder, where θ = 0°. The LES and the experimental data return similar locations for the flow separation point, 74.7° and 70.2° respectively, though the pressure levels returned by these models are somewhat different. The k-ε model predicts that the flow separates a lot later, beyond the 80° location, which is consistent with the under-estimation of the drag coefficient by this model. The location of the separation point predicted by the RSM model on the other hand, is much closer to that of the LES and the experimental data, which explains the improvements in the prediction of the value of the Drag coefficient, brought about by the introduction of this model. Under rotating conditions, the pressure distribution around the cylinder is no longer symmetric. The stagnation point is displaced by as much as 25° along the top surface at a spin ratio of 2, and, as indicated by the LES [10] data, at about the 90° location, over the top surface, the flow separates. Over the lower surface on the other hand, the pressure distribution returned by the LES data suggests that the flow remains attached over the entire lower surface of the rotating cylinder. The RSM predictions of the pressure distribution are in close agreement with those of the LES study, which is consistent with the earlier comparisons for the lift coefficient

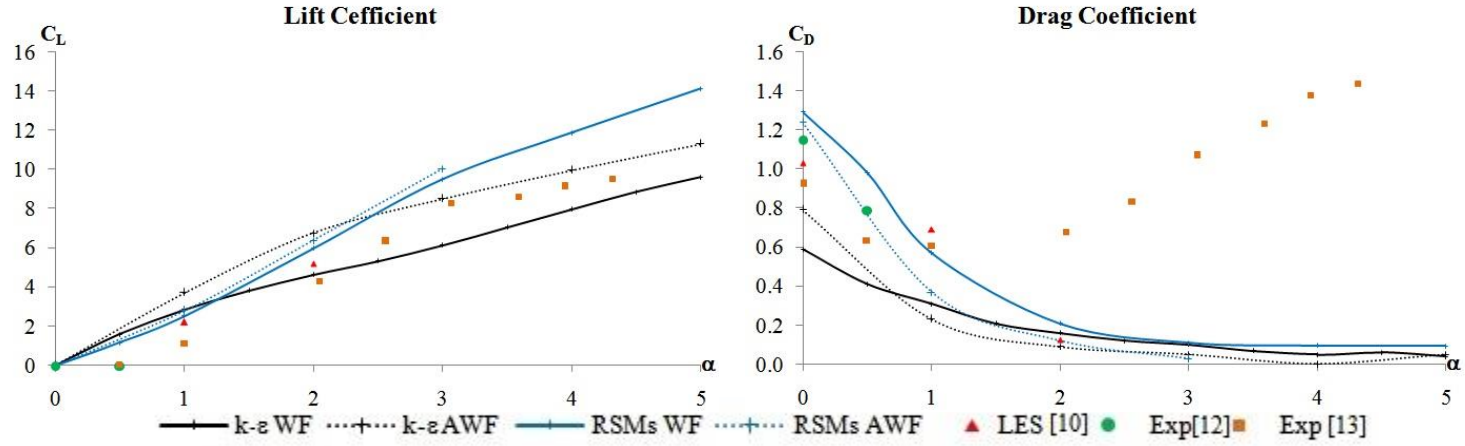

Fig. 2: The time-averaged prediction of aerodynamic (left) lift and (right) drag coefficient.

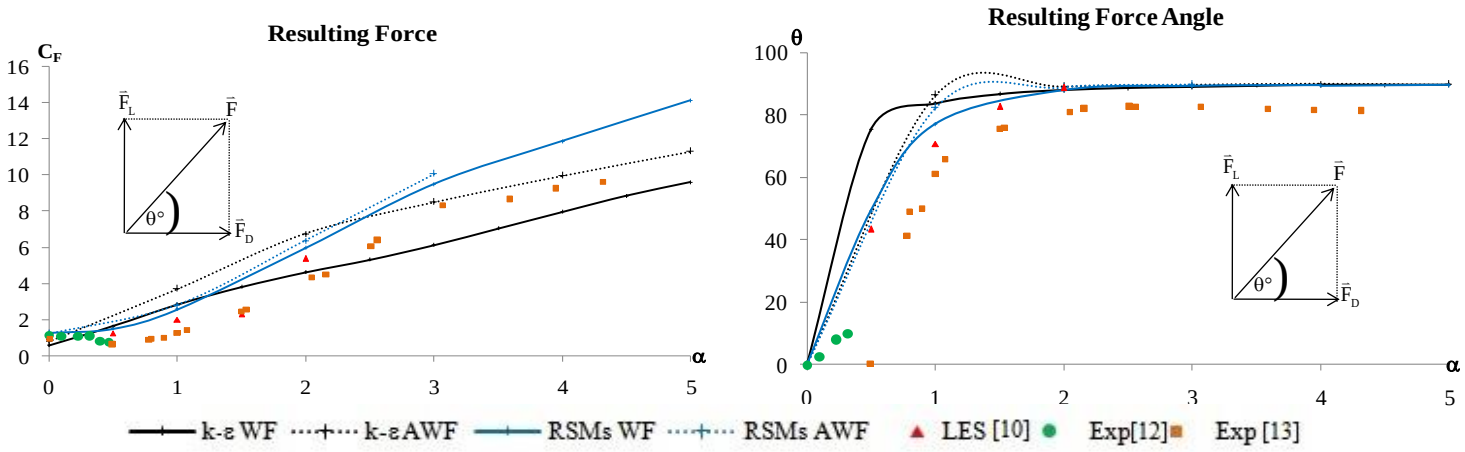

Fig. 3: The time-averaged prediction of (Left) Resulting force and (Right) direction.

Figure 5 illustrates the time-average streamlines of flow past a cylinder as a range of spin ratio up to 5. Entire streamlines are in good agreement with those obtained in pressure distribution as Figure 4. For flow past a stationary cylinder, the streamlines play a major role in symmetric along flow direction leading to obtain zero of lift coefficient. Whereas the embraced streamlines are presented in flow past a rotating cylinder. The rotation can dislocate the re-circulating flow from half back to upper cylinder shoulder, it seems that regions are smaller to smaller. In accordance with re-circulating flow position, the saddle point (*) where is the collection point of velocity branches also shifts in the same way. The position of stagnation (+), on the other hand translates in opposite rotating direction, consequently the lift coefficient is larger because it produces a more different pressure between upper and lower cylinder shoulders. Until spin ratios are beyond 4, the stagnation and saddle point move closing together resulting to be imbalance energy between potential (production) and kinetic (destruction) energy from both of those points. Therefore, streamlines are in

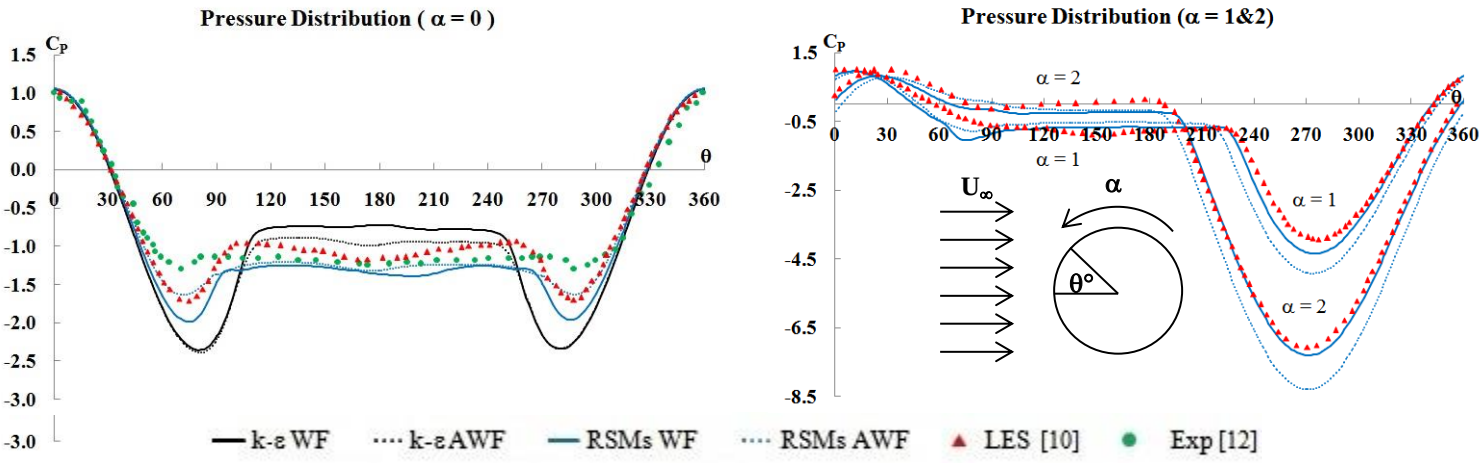

Fig. 4: The time-averaged pressure distribution of RSMs with WF as α = 0,1 and 2.

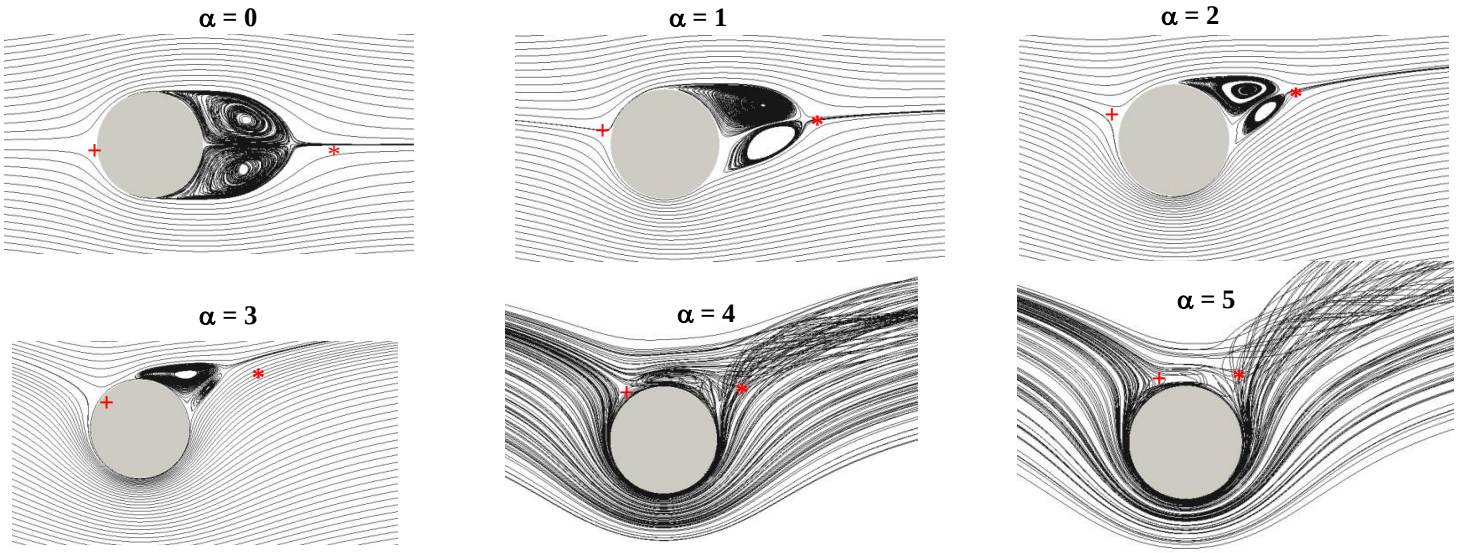

Fig. 5: The time-averaged streamline of RSMs with WF as α = 0,1,2,3,4 and 5.

The instantaneous flow plots of Figure 6 provide further information on the complexity and three-dimensionality of the flow. In the stationary case, the complexity of the flow path lines downstream of the cylinder suggests that the flow is highly unstable, due to strong vortex shedding behind the stationary cylinder. The flow over the front half of the stationary cylinder appears to be steady and symmetric. For the rotating case on the other hand, at a spin ratio of 2, the relative

simplicity of the flow field downstream of the rotating cylinder suggests that rotation stabilises the downstream flow. Flow separation is a lot more limited and vortex shedding is considerably weakened. The flow development over the rotating cylinder is non-symmetric and the main features are consistent with those suggested by the static pressure distributions of Figure 4.

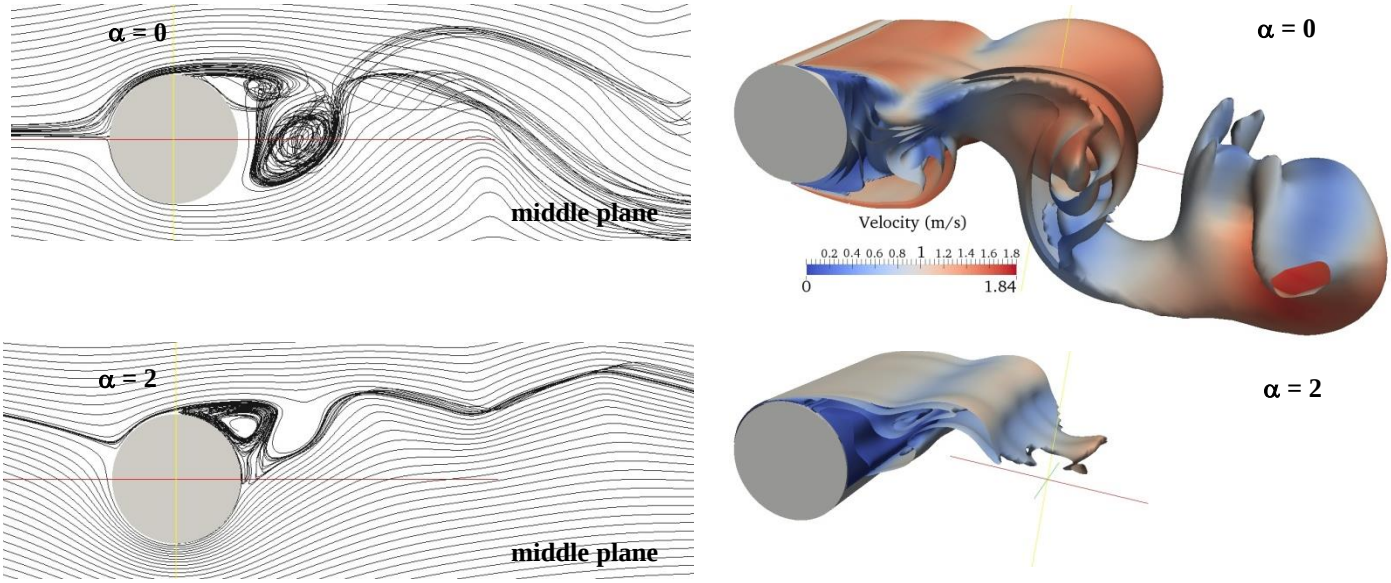

Fig. 6: (left) the streamline and (right) velocity level on k-iso-surface of RSMs with WF at t^* of a quarter vortex shedding period as α = 0 (top) & 2 (bottom).

5. Conclusion

This paper has presented predictions of three-dimensional and unsteady flows across stationary and rotating cylinders, using cost-effective high-Reynolds-number models of turbulence. It makes two main original contributions to our current knowledge. One is in the exploration of the effectiveness of different approaches to the high-Reynold-number modelling of the turbulent stresses and of the near-wall turbulence. The other is in the advancement of our understanding of the flow features present, which in turn explain the predictive strengths and deficiencies of the URANS models tested.

In the case of stationary cylinders, the two main flow characteristics which dominate the aerodynamic behaviour are the streamline curvature of the flow around the cylinder and the onset of flow separation near the 90^o location, which leads to an unsteady wake behind the cylinder. It is consequently no surprise that the resulting comparisons between predictions and experimental and LES data reveal that key parameters such as the drag coefficient and the frequency of vortex shedding can only be reliably predicted when the turbulent stresses are modelled through a second-moment closure and the wall-function strategy is more rigorous than the "standard" log-law-based approach.

In the case of rotating cylinder, as the spin ratio progressively increases, on the one hand the flow around the cylinder is no longer symmetric and the stagnation point is displaced in the direction opposite to the of the cylinder rotation, which leads to the development of a lift force. At the same time the downstream wake becomes progressively smaller as the spin ratio increases and eventually disappears, a development which leads to the disappearance of flow instabilities. As a result, while it is still necessary to employ a second-moment closure for the correct prediction of the aerodynamic parameters, the choice of wall-functions is no longer critical.

The main message is that unsteady three-dimensional flows across stationary and rotating cylinders can be reliably predicted using cost-effective high-Reynolds-number second-moment closures.

Acknowledgements

We would like to thank you the Royal Thai government for the research fund. And also, the Manchester Doctoral College Postgraduate Research (MDC PGR) conference fund for the supplement of the international conference fee.

References

[1] H. G. Magnus, *Ueber die Abweichung der Geschosse; und: ueber eine auffallende Erscheinung bei rotire; and on a remarkable phenomenon of rotating bodies*. Berlin: Taylor's Foreign Scientific Memoirs 804-10, 1853.

[2] M. Coutanceau and C. Ménard, "Influence of rotation on the near-wake development behind an impulsively started circular cylinder," *J. Fluid Mech.*, vol. 158, no. 191, p. 399, 1985.

[3] H. M. Badr and S. C. R. Dennis, "Time-dependent viscous flow past an impulsively started rotating and translating circular cylinder," *J. Fluid Mech.*, vol. 158, p. 447, 1985.

[4] S. Mittal and B. Kumar, "Flow past a rotating cylinder," *J. Fluid Mech.*, vol. 476, pp. 303-334, 2003.

[5] M. Brede, H. Eckelmann, and D. Rockwell, "On secondary vortices in the cylinder wake," *Phys. Fluids*, vol. 8, no. 8, p. 2117, 1996.

[6] M. Braza, P. Chassaing, and H. H. Minh, "Numerical study and physical analysis of the pressure and velocity fields in the near wake of a circular cylinder," vol. 166, 1986.

[7] V. A. Gushchin, A. V. Kostomarov, and P. V. Matyushin, "3D Visualization of the separated fluid flows," *J. Vis.*, vol. 7, no. 2, pp. 143-150, 2004.

[8] B. J. Cantwell and D. Coles, "An experimental study of entrainment and transport in the turbulent near wake of a circular cylinder," *J. Fluid Mech.*, vol. 136, no. 1983, p. 321, 1983.

[9] C. Norberg, "EFFECTS OF REYNOLDS NUMBER AND A LOW-INTENSITY FREESTREAM TURBULENCE ON THE FLOW AROUND A CIRCULAR CYLINDER," 1987.

[10] S. J. Karabelas, "Large Eddy Simulation of high-Reynolds number flow past a rotating cylinder," *Int. J. Heat Fluid Flow*, vol. 31, no. 4, pp. 518-527, 2010.

[11] S. J. Karabelas, B. C. Koumroglou, C. D. Argyropoulos, and N. C. Markatos, "High Reynolds number turbulent flow past a rotating cylinder," *Appl. Math. Model.*, vol. 36, no. 1, pp. 379-398, 2012.

[12] K. Aokii and T. Ito, "Flow Characteristics around a Rotating Cylinder," 2001.

[13] E. G. Reid, "Tests of Rotating Clinders," *Tech. Notes Natl. Advis. Comm. Aeronaut.*, vol. 209, 1924.

[14] W. M. Swanson, "The Magnus Effect: A Summary of Investigation to Date," *ASME, J. Basic Eng.*, vol. 83, pp. 461-470, 1961.

[15] B. R. Clayton, "BWEA Initiative on wind assisted ship propulsion (WASP)," *J. Wind Eng. Ind. Aerodyn.*, vol. 19, pp. 251-276, 1985.

[16] T. J. Craft, H. Iacovides, and B. E. Launder, "Dynamic Performance of Flettner Rotors With and Without Thom Discs," *Tsfp7*, vol. 12, pp. 1-6, 2011.

[17] A. Travin, M. Shur, M. Strelets, and P. Spalart, "Detached-Eddy Simulations Past a Circular Cylinder," *Flow Turbul. Combust.*, vol. 63, pp. 293–313, 1999.

[18] A. Elmiligui, K. Abdol-Hamid, S. Massey, and S. Pao, "Numerical Study of Flow Past a Circular Cylinder Using RANS, Hybrid RANS /LES and PANS Formulations," *22nd Appl. Aerodyn. Conf. Exhib.*, pp. 1-18, 2004.

[19] B. J. Daly and F. H. Harlow, "Transport equation in turbulence," *Phys. Fluids*, vol. 13, pp. 2634-2649, 1970.

[20] M. M. Gibson and B. E. Launder, "Ground effects on pressure fluctuations in the atmospheric boundary layer," *J. Fluid Mech.*, vol. 88, pp. 491-511, 1978.

[21] T. J. Craft, A. V. Gerasimov, H. Iacovides, and B. E. Launder, "Progress in the generalization of wall-function treatments," *Int. J. Heat Fluid Flow*, vol. 23, no. 2, pp. 148-160, 2002.

[22] F. S. Lien and M. A. Leschziner, "A pressure-velocity solution strategy for compressible flow and its application to shock/boundary-layer interaction using second-moment turbulence closure," *J. Fluids Eng.*, vol. 115, pp. 717-725, 1993.